

Safety Properties and Collision Behavior of Robotic Arms with Elastic Tendon Actuation

Thomas Lens*, Oskar von Stryk

Simulation, Optimization and Robotics Group, Technische Universität Darmstadt, Germany

[lens,stryk]@sim.tu-darmstadt.de

Andreas Karguth

TETRA Gesellschaft für Sensorik, Robotik und Automation, Ilmenau, Germany

Abstract

Applications with physical human-robot interaction require a high level of safety even in case of software or hardware failures. This paper highlights the advantages of combining tendon actuation with transmission elasticity to maximize safety for robotic arms sharing workspaces with humans. To this end, the collision behavior of combinations of tendon or joint and elastic or stiff actuation with geared electrical motors as reliable actuators is compared using the lightweight BioRob arm as robotic platform in simulation. For the comparison a worst case scenario is assumed in which the robot arm is accelerated with maximum supply voltage over its joint range and collides with maximum end-effector velocity. The study shows that the robot arm achieves end-effector velocities as high as 6 m/s and that elastic tendon actuation reduces the end-effector impact energy and force by up to 90 % compared to stiff joint actuation. A considerable reduction of the gearbox stress is also achieved. In addition, the effect of motor current fuses limiting the motor torques is evaluated. It is shown that for the given high speed scenario, torque limiting devices can be effective to prevent excessive clamping forces in case of failure, but can not reduce the impact peak force without heavily compromising the robot dynamics. The main design criterion for safety should therefore be lightweight link design and compliant actuation, which can be achieved by using elastic tendon actuation. The paper concludes with the comparison of safety properties of robotic arms in research and industry.

1 Introduction

Many efforts are taken to increase safety for applications with physical human-robot interaction (pHRI) and a number of capable demonstrators have been presented over the last years. Some of the research places focus on enabling active safety for conventional robotic arms using sensor based collision avoidance or collision detection and reaction methods. But the certification of safety is a huge challenge, because it requires high levels of safety for humans sharing the workspace of the robot even in case of hardware or software failures.

Beyond safety from injuries perceived safety and convenience play also a very important psychological role in applications with pHRI. Because of the hardware limitation regarding safety of conventionally built robots, especially in case of high velocities, clamping situations, or hard- and software failures, new actuation designs for increased passive safety are being developed. One of the main design goals is meeting the strict safety requirements of pHRI applications without compromising performance.

Lightweight design and compliant actuators are now

widely seen as key features. Elasticity can be realized by using inherently compliant actuators, such as artificial pneumatic muscles [1,2] or by using elastic elements in series with standard geared motors [3]. Additional actuators can be used to adapt stiffness or damping [4–6] or to combine actuators with complementary features [7]. For conventional and heavy actuators the robot arm inertia can be reduced in favor of lightweight design by using cable actuation instead of placing the motors in or near the joints [8].

The BioRob arm combines tendons and elasticity in the drivetrain to achieve both lightweight design and compliant actuation [9]. This paper compares the collision behavior and safety properties of the elastic tendon actuation as used in the BioRob arm to other actuation designs. **Section 2** describes the properties of elastic tendon actuation. A worst case collision scenario is defined in **Section 3**. After introducing all possible combinations of elastic or stiff, and tendon or joint actuation in **Section 4**, the impact behavior of the actuation designs is evaluated in **Section 5** with respect to impact energy, force and joint torques using the worst case scenario. In addition, the effect of fuses limiting the motor currents on the impact properties of the

*Corresponding author

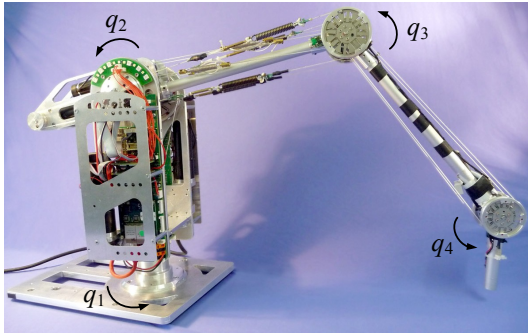


Figure 1: BioRob-X4 arm with elastic tendon actuation in all four joints.

robot arm is examined to clarify if additional safety is obtained by these components.

The paper concludes with a comparison of the effective operational space masses of the evaluated actuation designs when used in the BioRob arm and of effective mass values reported in literature for several robotic arms.

2 Elastic Tendon Actuation

The actuation approach of the BioRob arm as shown in **Figure 1** aims at combining the robust behavior of standard electrical motors with the safety characteristics of elasticity in the drivetrain and a radical lightweight design by using tendons to actuate the robot joints [10].

When using tendons spanning multiple joints, additional friction is introduced. However, this comes with several advantages. By using tendons, the motors can be placed near the base, thus reducing the robot arm's inertia, or can even be used as a counterbalance for the weight of the links. The reduction of mass and inertia allows to use smaller and less heavy motors and gears. In addition, by using elasticity in the tendons, the reflected rotor inertia and friction are dynamically decoupled from the link side, reducing shocks on the gearbox as well as on the environment in case of a collision.

These properties will be quantified and compared in detail to other actuation designs in the following sections.

3 Collision Trajectory

In the worst case a software or hardware failure can cause the motor input voltages to be permanently set to the maximum supply voltage. The trajectory chosen for collision evaluation is depicted in **Figure 2** and **Figure 3**. The robot arm starts in a configuration near the mechanical joint limits to have a maximum acceleration distance and accelerates to the opposing joint limits with the maximum voltage, where the end-effector collides with the object marked in grey. The maximum motor input voltage of the BioRob arm is $U_{a,max} = 12 \text{ V}$.

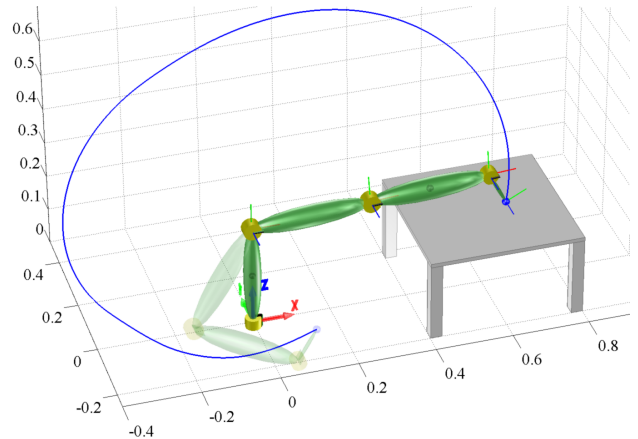


Figure 2: Simulated collision trajectory of the BioRob arm, shown in initial configuration (transparent rendering) and configuration just before impact with the grey object (solid rendering). Axis dimensions are given in meters.

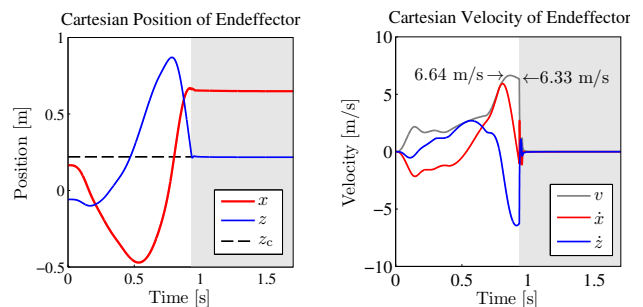


Figure 3: End-effector trajectory in Cartesian space. The collision occurs at $z_c = 0.22 \text{ m}$. The collision phase is marked in grey.

The highest end-effector velocities and lever arms are achieved in the outstretched configuration. The last link does not significantly contribute to the end-effector velocity because of its short length. In case of elastic actuation it has the potential to decouple the rest of the robot arm from the collision during the first impact phase, causing a significant decrease of the impact force peak.

Higher impact forces can therefore be expected when reducing the effective collision force lever arm of the last link by pointing the link towards the collision surface normal. The chosen impact configuration is shown in **Figure 2**.

The activation of the maximum motor voltages is timed separately in each motor in order to reach the described impact configuration. The motor of the second joint is accelerated from the beginning of the trajectory, whereas the motors of the third and fourth joint are accelerated at a later stage of the trajectory.

As can be recognized from **Figure 3**, the end-effector velocity at time of impact $v_c = 6.33 \text{ m/s}$ is slightly lower than the maximum trajectory velocity of $v = 6.64 \text{ m/s}$, which is in turn lower than the maximum achievable end-effector velocity in the outstretched configuration of $v = 7.4 \text{ m/s}$.

Table 1: Model parameters of the BioRob-X4 arm without gripper: Denavit-Hartenberg parameters DH, link center of mass position r_c with respect to the coordinate system in the subsequent joint, link mass m , combined transmission ratio z , rotor inertia I_r , and transmission stiffness k_e and damping d_e , both with respect to the joint.

Joint	1	2	3	4
DH (d, a, α)	(0.276, 0, $\frac{\pi}{2}$)	(0, 0.307, 0)	(0, 0.310, 0)	(0, 0.17, 0)
r_c [m]	(0, -0.14, 0)	(-0.32, 0, 0)	(-0.16, 0, 0)	(-0.07, 0, 0)
m [kg]	2.350	1.530	0.160	0.055
z [-]	73.6	80.0	47.0	52.8
I_r [kgm ²]	$3.33 \cdot 10^{-6}$	$3.33 \cdot 10^{-6}$	$3.33 \cdot 10^{-6}$	$1 \cdot 10^{-6}$
k_e [Nm/rad]	100	80	35	6
d_e [Nms/rad]	0.05	0.05	0.05	0.05

Nevertheless, for the stated reasons, the highest impact forces can be expected with the described configuration, as was validated in simulation.

When using elastic actuation, the joint velocity can be significantly higher than the motor velocity. These effects are discussed in the next sections. The consequences on the selection of a worst case trajectory are beyond the scope of this paper and are subject of future research.

4 Evaluated Actuation Designs

For the comparative simulation several different actuation designs are to be defined. All designs are based on the parameters of the BioRob-X4 arm, as listed in **Table 1**, and combine tendon or joint with elastic or stiff actuation.

The first group of actuation designs uses *Elastic Tendon Actuation* (ETA) with various stiffness settings:

- (a) ETA with low tendon stiffness k_e and damping d_e as used in the BioRob-X4 arm (cf. Table 1),
- (b) ETA with medium stiffness $8 \cdot k_e$ and damping $8 \cdot d_e$,
- (c) ETA with high stiffness $80 \cdot k_e$ and damping $80 \cdot d_e$.

In the case of infinite stiffness and damping, the ETA transforms into *Stiff Tendon Actuation* (STA), which is not practically implementable because of the inherent elasticity of tendons and belts, but nevertheless interesting from a theoretical point of view to determine the upper bound behavior of ETA with high stiffness:

- (d) STA with stiff coupling between motor and joint.

The last two defined actuation designs used for comparison have the motors placed in the joints instead of using tendon actuation. The first design uses a series elastic transmission element between motor and joint, the *Elastic Joint Actuation* (EJA):

- (e) EJA with motors placed in the joints.

The second design, *Stiff Joint Actuation* (SJA), exhibits stiff coupling between motor and joint:

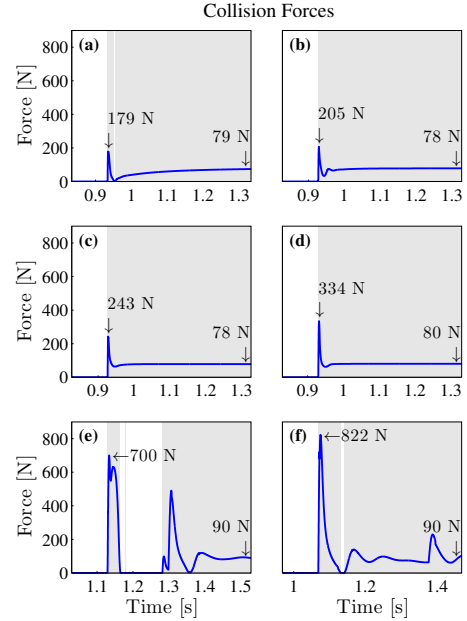


Figure 4: End-effector collision forces for (a)–(c) ETA, (d) STA, (e) EJA, and (f) SJA (cf. Section 4).

(f) SJA with stiff coupling of motors and links.

To achieve realistic results, the collision area is modeled with the stiffness of the human neck, which represents one of the safety-critical areas of the human body. The contact is modeled as Hunt-Crossley material with a combined contact stiffness of $k_{coll} = 10^4 \text{ N/m}$, the stiffness of the human neck area as given in [11], and a nonlinear damping parameter of $\lambda_{coll} = 5 \cdot 10^3 \text{ Ns/m}^2$. For details on the contact model we refer to [12].

5 Impact Evaluation

5.1 Impact without Current Limitation

The resulting end-effector collision forces are displayed in **Figure 4** and range from a peak force of 179 N for the BioRob-X4 arm using ETA with the lowest stiffness to 822 N for the same robot arm structure with SJA instead of elastic cable actuation, i.e. with the motors located in the joints and rigidly connected to the links.

The static clamping forces after the first impact peak are generated by the maximum actuator torques and the gravitational torques of the robot structure and depend on the current robot configuration. For the designs (a)–(d) with cable actuation, the static clamping force is about 80 N, for the designs (e)–(f) with joint actuation the additional gravitational forces by placing the motors in the joints amount to a higher static clamping force of 90 N.

As can be seen in **Figure 5**, designs (a)–(d) have roughly the same kinetic energy

$$E_{kin} = E_{kin,links} + E_{kin,motors} \quad (1)$$

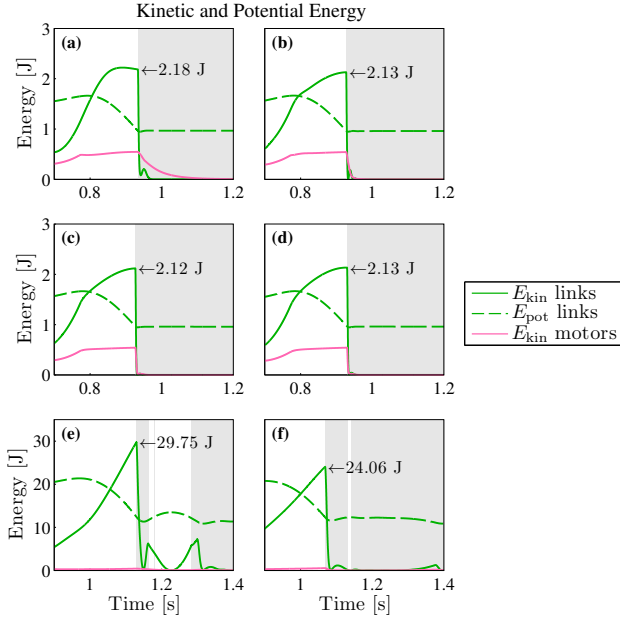


Figure 5: Kinetic and potential energies for (a)–(c) ETA, (d) STA, (e) EJA, and (f) SJA (cf. Section 4).

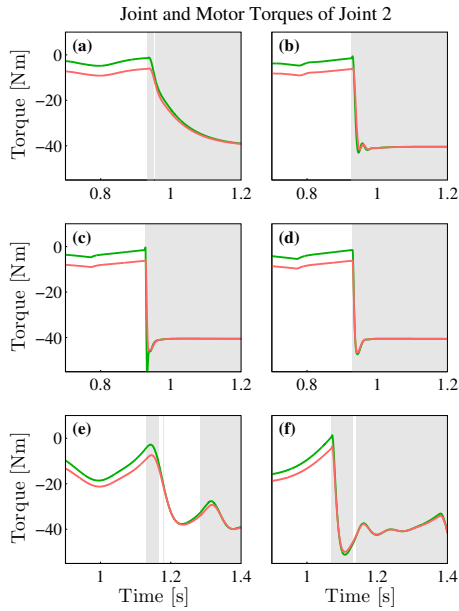


Figure 6: Collision Torques of joint two for (a)–(c) ETA, (d) STA, (e) EJA, and (f) SJA (cf. Section 4).

at impact time. The designs with lower actuation stiffness, however, possess a less strong coupling between motors and links, which acts as a low pass filter on shocks from the links to the motors. For that reason the actuators with low stiffness coupling exhibit a higher decay time constant of the kinetic energy of the motors, as can be seen in Figure 5, causing a decrease of peak impact force from (d) 334 N in case of stiff coupling to (a) 179 N in case of low stiffness coupling (cf. Figure 4).

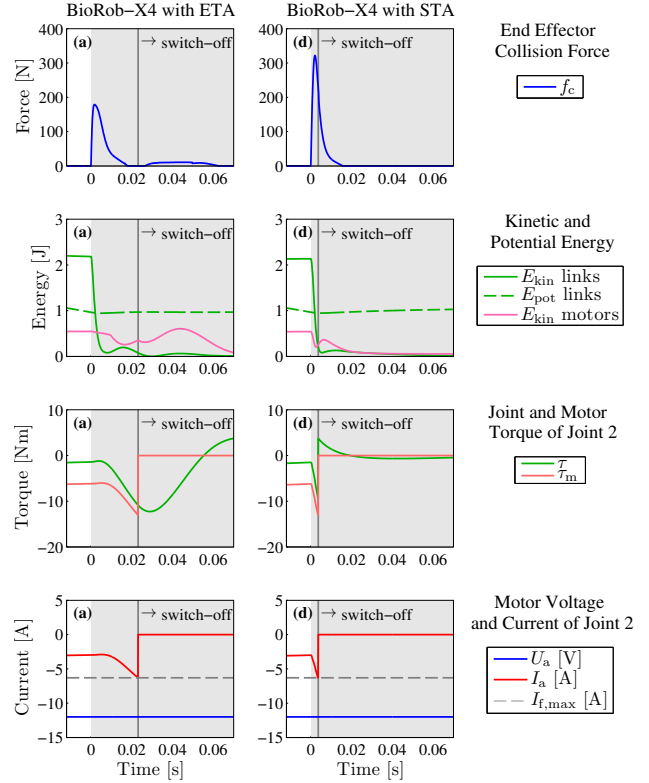


Figure 7: Comparison of the collision behavior of the BioRob-X4 arm with elastic tendon actuation (ETA) (a) and stiff tendon actuation (STA) (b) using ideal fuses with switch-off current $I_{f,max} = 6.3$ A.

Placing the motors in the joints, as in designs (e) and (f) with joint actuation, results in a shift of masses towards the end-effector increasing the inertia and therefore also the kinetic energy of the robot arm from about 2 J to 24 J for stiff transmission and 30 J for series elastic transmission. The increase in kinetic energy of these designs leads to significantly higher impact forces. The impact kinetic energy with elastic transmission (e) is higher than with stiff transmission (f) because the elastic decoupling of motors and joints enables independent joint dynamics with much higher joint velocities. This effect is also visible when comparing the kinetic energy of elastic tendon (2.18 J) and stiff tendon actuation (2.13 J), although less distinct because of the lower link masses.

In contrast to the impact forces and energies the dominant factor on the joint torques is the transmission elasticity (cf. Figure 6). Low actuation transmission stiffness, such as for designs ETA (a) and EJA (e), low pass filter the collision shock on the motors and gearboxes.

5.2 Impact with Current Limiting Fuses

This section examines if the effects of the collision scenario presented in the previous sections can be attenuated by limiting the joint torques using robust hardware safety shut-off devices. For the given lightweight arm a decou-

Table 2: Effective end-effector mass $\Lambda_{c,z}$ in normal and $\Lambda_{c,x}$ in tangential collision direction, and maximum effective mass $\Lambda_{c,xz}$ in the trajectory plane at impact time for the 4 DOF BioRob arm with elastic tendon actuation (ETA), stiff tendon actuation (STA), elastic joint actuation (EJA), and stiff joint actuation (SJA).

	ETA	STA	EJA	SJA
$\Lambda_{c,x}$ [kg]	0.009	0.239	0.119	0.471
$\Lambda_{c,z}$ [kg]	0.023	0.155	0.306	0.755
$\Lambda_{c,xz}$ [kg]	0.122	0.521	1.66	1.86

ling of those joints for which the maximum joint torque is exceeded without using brakes is feasible without compromising safety. This can be realized using a clutch-like device on joint level or motor fuses limiting the motor currents.

A comparison of the effects of the fuses on the collision forces and joint torques for elastic and stiff tendon actuation is shown in **Figure 7**. Ideal fuses with the lowest possible shut-off current of 6.3 A were chosen. Lower shut-off currents would overly restrict the dynamics of the robot arm and are therefore not suitable.

The fuse in the second joint blows at 23 ms for the elastic tendon actuation, and at 3.6 ms for the stiff tendon actuation. In neither cases a reduction of the impact peak force is achieved. As mentioned, the fuse switch-off current is at the lowest acceptable level. The switch-off delays therefore cannot be further reduced.

However, the joint torque τ and motor torque τ_m are bounded (to 13 Nm in the second joint) and the clamping force is reduced to zero. Fuses can therefore be used to prevent clamping in case the control software fails to do so. In normal operation, however, the controller is able to switch off the motors by software. Therefore, hardware based switch-off devices are only needed in the exceptional case of failure. To avoid additional complexity and weight, electrical fuses are therefore more practical for the presented setting than mechanical devices in the joints limiting the joint torques.

5.3 Comparison of Effective Mass

All simulated actuation designs used the same collision trajectory and roughly had the same impact velocity and configuration. Therefore, the effective end-effector mass in operational space can be an appropriate measure for safety comparison. The effective mass is calculated by transforming the joint level dynamics equations to operational space [13]. **Table 2** lists the effective end-effector mass of all actuation designs at time of impact.

For comparison, effective mass values reported in literature are listed in **Tables 3** and **4**. Because the inertia strongly depends on the robot configuration, each table stands for a distinct robot configuration as reported in the respective sources. For better comparability the normalized effective

Table 3: Comparison of effective end-effector mass for the configuration shoulder $q_S = 20^\circ$ and elbow $q_E = -90^\circ$ (cf. [7]). Values marked with * are taken from [7].

	DOF	Reflected Inertia	Payload	Normalized Eff. Mass
BioRob-X4	4	0.344 kg	20 N	0.017 kg/N
Stanford S2 ρ	1	0.98 kg *	30.6 N *	0.032 kg/N *
human arm	7	2.11 kg *	62 N *	0.030 kg/N *
Stanford DM ²	3	3.51 kg *	60 N *	0.060 kg/N *
PUMA560	6	24.88 kg *	21.6 N *	1.15 kg/N *

Table 4: Comparison of effective end-effector mass in collision direction for the configuration shoulder $q_S = 0^\circ$, elbow $q_E = 0^\circ$, and wrist joint $q_W = -90^\circ$ (cf. [14]). Values marked with † are taken from [14], values with ‡ from [15].

	DOF	Reflected Inertia	Payload	Normalized Eff. Mass
BioRob-X4	4	0.104 kg	20 N	0.005 kg/N
DLR LWR 3	7	4 kg †	147 N ‡	0.027 kg/N

mass [7] is also listed. For the human arm a payload for repeated manipulations is assumed.

6 Conclusions

The study shows for the evaluated collision scenario with the BioRob-X4 robot arm that elastic tendon actuation reduces the kinetic impact energy by 90 % to 2 J, the effective end-effector mass by 93 % to 122 g, the dynamic impact force by 80 % and the static clamping force by 10 % compared to stiff joint actuation of the same robot. A reduction of the impact torque shocks acting on the gearboxes is also achieved. These improvements are due to the tendon actuation enabling the motor placement at the first link and at a balancing position in the second link and by the transmission elasticity decoupling the motor from the link inertia.

By this means the robot arm exhibits a high level of safety even at velocities as high as 6 m/s. At the outstretched configuration, the robot arm has an effective mass of only 100 g and remains below 0.5 kg throughout the workspace excluding regions close to singular configurations.

The effective end-effector mass of 1.66 kg for elastic joint actuators compared to 122 g for elastic tendon actuators demonstrates that a major portion of the maximum payload of 20 N is needed to support the robot structure when using elastic actuators with motors placed in the joints. In case of elastic tendon actuators, the weight of the distant links is reduced and counterbalanced, such that only a minimal portion of the maximum payload is required to overcome the gravitational forces.

The evaluation of the effect of motor current limiting fuses

showed that the peak impact force can not be reduced without imposing major limitations on the robot arm dynamics. This holds for general joint torque limiting devices when used in the presented scenario and high velocities. However, clamping forces and joint torques can be limited by these devices in order to protect the hardware and environment from excessive stress caused by clamping in case the control software fails. Therefore, motor current fuses are sufficient and even beneficial compared to mechanical joint torque limitation devices by saving weight and complexity. With elastic tendons, the torque shocks after a fuse switch-off are low pass filtered and are not reversed abruptly as in the case of stiff actuation, again being protective for the hardware.

In summary, elastic tendon actuation can enable excellent safety properties for high speed pHRI applications with high safety requirements by reducing the link inertia and decoupling motors and links.

Not covered in detail in this evaluation is the fact that elastic actuation can store energy and can lead to significantly higher joint than motor velocities. The simulation results indicate that the negative effect of elastic actuation on the collision properties is much lower in case of elastic tendon actuation with only a 2 % increase in kinetic energy, compared to elastic joint actuation with an increase of 19 %, at least for the unloaded state. Future work will concentrate on this topic in more detail.

Acknowledgments

The research presented in this paper was supported by the German Federal Ministry of Education and Research BMBF under grant 01 RB 0908 A.

References

- [1] A. Bicchi and G. Tonietti, "Fast and "soft-arm" tactics," *IEEE Robot. Autom. Mag.*, vol. 11, no. 2, pp. 22–33, 2004.
- [2] M. Van Damme, B. Vanderborght, B. Verrelst, R. Van Ham, F. Daerden, and D. Lefeber, "Proxy-based sliding mode control of a planar pneumatic manipulator," *Int. J. Robotics Research*, vol. 28, no. 2, pp. 266–284, 2009.
- [3] G. Pratt and M. Williamson, "Series elastic actuators," *Proc. IEEE/RSJ Int. Conf. Intelligent Robots and Systems*, vol. 1, p. 399, 1995.
- [4] R. Schiavi, G. Grioli, S. Sen, and A. Bicchi, "VSA-II: a novel prototype of variable stiffness actuator for safe and performing robots interacting with humans," in *Proc. IEEE Int. Conf. Robotics and Automation*, 2008, pp. 2171–2176.
- [5] R. Van Ham, T. Sugar, B. Vanderborght, K. Hollander, and D. Lefeber, "Compliant actuator designs," *IEEE Robot. Autom. Mag.*, vol. 16, no. 3, pp. 81–94, 2009.
- [6] A. Albu-Schäffer, S. Wolf, O. Eiberger, S. Haddadin, F. Petit, and M. Chalon, "Dynamic modelling and control of variable stiffness actuators," in *Proc. IEEE Int. Conf. Robotics and Automation*, 2010, pp. 2155–2162.
- [7] D. Shin, I. Sardellitti, Y.-L. Park, O. Khatib, and M. Cutkosky, "Design and control of a bio-inspired human-friendly robot," *Int. J. Robotics Research*, vol. 29, no. 5, pp. 571–584, 2010.
- [8] B. Rooks, "The harmonious robot," *Industrial Robot: Int. J.*, vol. 33, pp. 125–130, 2006.
- [9] T. Lens, J. Kunz, C. Trommer, A. Karguth, and O. von Stryk, "Biorob-arm: A quickly deployable and intrinsically safe, light-weight robot arm for service robotics applications," in *Proc. 41st Int. Symp. Robotics / 6th German Conf. Robotics*, 2010.
- [10] T. Lens, J. Kunz, and O. von Stryk, "Dynamic modeling of the 4 DoF BioRob series elastic robot arm for simulation and control," in *Simulation, Modeling, and Programming for Autonomous Robots*, ser. Lecture Notes in Artificial Intelligence. Springer, 2010, pp. 411–422.
- [11] (2011, Feb.) BG/BGIA risk assessment recommendations according to machinery directive - design of workplaces with collaborative robots. BGIA – Institute for Occupational Safety and Health of the German Social Accident Insurance. [Online]. Available: http://www.dguv.de/ifa/en/prakollaborierende_roboter/index.jsp
- [12] T. Lens, K. Radkhah, and O. von Stryk, "Simulation of dynamics and realistic contact forces for manipulators and legged robots with high joint elasticity," in *Proc. 15th Int. Conf. Advanced Robotics*, 2011, pp. 34–41.
- [13] O. Khatib, "Inertial properties in robotic manipulation: An object-level framework," *Int. J. Robotics Research*, vol. 14, no. 1, pp. 19–36, 1995.
- [14] S. Haddadin, A. Albu-Schäffer, and G. Hirzinger, "Requirements for safe robots: Measurements, analysis and new insights," *Int. J. Robotics Research*, vol. 28, no. 11-12, pp. 1507–1527, 2009.
- [15] DLR Light-Weight Robot LWR III data sheet. DLR. [Online]. Available: http://www.dlr.de/rm/Portaldata/52/Resources/dokumente/light_weight_robot/dlr-lbriii-eng_homepage.pdf